BNL-212013-2019-JAAM

Efficient Light Harvesting Biotic-Abiotic Nanohybrid System Incorporating Atomically Thin van der Waals Transition Metal Dichalcogenides

M. Li, M. Cotlet

To be published in "ACS Photonics"

April 2019

Center for Functional Nanomaterials

Brookhaven National Laboratory

U.S. Department of Energy

USDOE Office of Science (SC), Basic Energy Sciences (BES) (SC-22)

Notice: This manuscript has been authored by employees of Brookhaven Science Associates, LLC under Contract No. DE-SC0012704 with the U.S. Department of Energy. The publisher by accepting the manuscript for publication acknowledges that the United States Government retains a non-exclusive, paid-up, irrevocable, world-wide license to publish or reproduce the published form of this manuscript, or allow others to do so, for United States Government purposes.

DISCLAIMER

This report was prepared as an account of work sponsored by an agency of the United States Government. Neither the United States Government nor any agency thereof, nor any of their employees, nor any of their contractors, subcontractors, or their employees, makes any warranty, express or implied, or assumes any legal liability or responsibility for the accuracy, completeness, or any third party's use or the results of such use of any information, apparatus, product, or process disclosed, or represents that its use would not infringe privately owned rights. Reference herein to any specific commercial product, process, or service by trade name, trademark, manufacturer, or otherwise, does not necessarily constitute or imply its endorsement, recommendation, or favoring by the United States Government or any agency thereof or its contractors or subcontractors. The views and opinions of authors expressed herein do not necessarily state or reflect those of the United States Government or any agency thereof.

Efficient light harvesting biotic-abiotic nanohybrid system incorporating atomically thin van Der Waals transition metal dichalcogenides

Mingxing Li, Jia-Shiang Chen and Mircea Cotlet*

Center for Functional Nanomaterials, Brookhaven National Laboratory, Upton New York 11973

E-mail: cotlet@bnl.gov

Abstract. Inspired by nature's light harvesting complex architectures, which bring together, in one unit, several active nanocomponents to harvest light and to flow the harvested energy in precise directions and places, we designed and assembled a biotic/abiotic step-wise energy transfer nanohybrid system which is based on an atomically thin, two-dimensional (2D) van Der Waals semiconductor, colloidal quantum dots and a light harvesting protein. We utilized the van Der Waals semiconductor as a 2D platform for bottom-up assembly, connecting nanocomponents via electrostatic self-assembly and layer-by-layer polyelectrolyte deposition. Through bandgap engineering of the self-assembled active components, we created conditions for efficient directional stepwise energy transfer, from optically excited quantum dots, to proteins and finally to the 2D van Der Waals semiconductor, here molybdenum diselenide ($MoSe_2$). A field effect transistor incorporating the biotic/abiotic nano hybrid was demonstrated to exhibit enhanced spectral responsivity when compared to the pristine device (2D van Der Waals semiconductor only). This is because the biotic/abiotic nano hybrid exhibits enhanced absorption cross section and enhanced light harvesting through the addition of quantum dots and proteins next to $MoSe_2$, which in turn leads to enhanced exciton generation in $MoSe_2$ via energy transfer from quantum dots to proteins and finally to $MoSe_2$.

Keywords: biotic-abiotic complex, nanobio devices, energy transfer, van Der Waals materials, allophycocyanin, quantum dots, self-assembly.

A biotic/abiotic nanodevice incorporates elements of biology, for example DNA, enzymes or proteins, inorganic, organic and/or metal components. In designing a biotic/abiotic nanodevice, we often inspire from nature's complex and precisely assembled nanoarchitectures. A well know example of such a nanoarchitecture is the natural light harvesting complex, a collection of chromophores of different spectral signatures which are capable to harvest light across the UV-visible range and to interact strongly via energy hopping and directional energy transfer, with transfer efficiencies approaching unity.[1-4] Inspired from nature's light harvesting complexes, we assembled a biotic-abiotic nanohybrid structure which has the potential to be utilized in solar energy harvesting. In our design, we use an atomically thin, two-dimensional (2D) van Der Waals semiconductor[5-8] as the starting platform for the assembly of the nanohybrid (Figure 1a). Atomically thin 2D van Der Waals semiconductors exhibit high surface to volume aspect ratio, a property which is extremely suitable for bottom up self-assembly. Furthermore, we use $MoSe_2$ as a 2D van Der Waals semiconductor which is known to exhibit indirect to direct energy bandgap inversion when its thickness reduces from bulk crystal to monolayer. It also exhibits high in-plane carrier mobility due to its atomically thin thickness.[5-6] These properties are extremely appealing for solar and photodetector applications. In this present work we combined $MoSe_2$ with two other light harvesting nanostructures, inorganic colloidal quantum dots and the protein allophycocyanin (APC)[9-10]. Through electrostatic self-assembly and energy bandgap engineering, we demonstrate for the first time a biotic/abiotic light harvesting nanohybrid functioning via multi-step cooperative energy transfer among nanocomponents. The assembled nanohybrid exhibits enhanced light harvesting, exciton and carrier generation, properties which aid toward increased photoresponsivity when this biotic-abiotic nanostructure is incorporated in a field effect transistor.

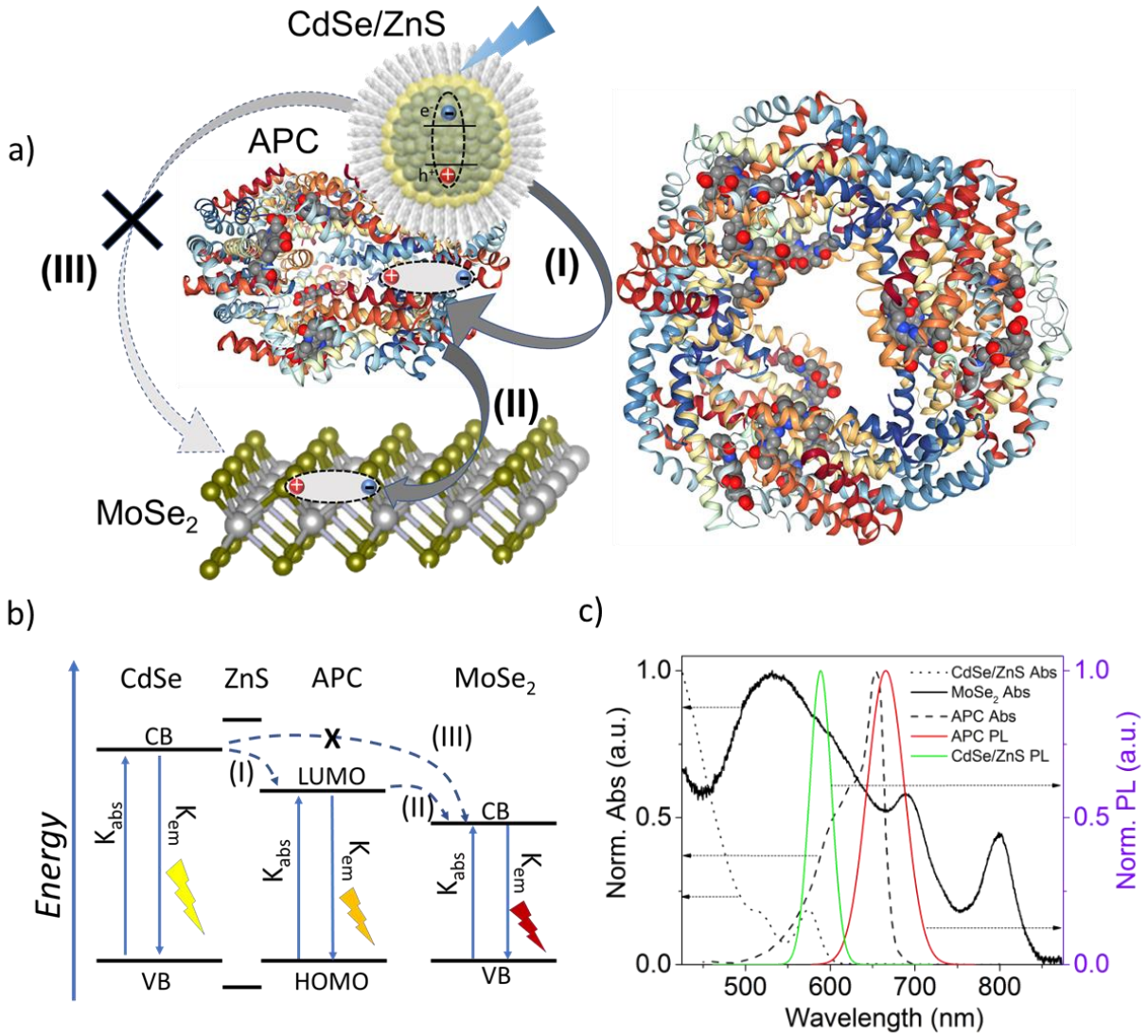

Figure 1. (a) Cartoon depicting the biotic/abiotic hybrid nanostructure composed of an atomically thin $MoSe_2$ nanosheet, colloidal core/shell CdSe/ZnS quantum dot (QD) and the light harvesting protein allophycocyanin (APC). APC structure was generated with RCSB PDB with crystal data from ref. [11] Also shown is a top view of the trimeric APC with phycocyanobilin chromophores drawn as grey balls. (b) energy band diagram shows possible types of light stimulated interactions in the proposed biotic/abiotic hybrid nanostructure. Full lines indicate radiative transitions, dashed lines indicate possible paths for non-radiative FRET. Cross in both a) and b) indicates inhibited energy transfer from QD directly to $MoSe_2$ by the large separation distance provided by APC (see text for discussion). (c) absorption and emission properties of various components constituting the biotic/abiotic hybrid nanostructure (PL, photoluminescence, Abs, absorption). For $MoSe_2$, the absorption spectrum is that of a monolayer. A 440 nm laser light was used to excite QDs, while a 532 nm laser light was used to excite APC.

The proposed nanoarchitecture is shown in Figure 1a, while a detailed design for the same architecture is shown in Figure 2. The biotic-abiotic hybrid nanostructure contains an atomically thin $MoSe_2$ flake (monolayer to few layers) as the bottom platform. While $MoSe_2$ transitions from

an indirect energy bandgap semiconductor at bulk crystal to direct bandgap semiconductor at monolayer, with monolayer $MoSe_2$ exhibiting strong photoluminescence with a peak at 809 nm (Figure.1b, dark red), bilayer and trilayer $MoSe_2$ also exhibit strong photoluminescence, with peaks at 792 nm and 765 nm, respectively.[5] $MoSe_2$ absorption spans a large breath of the UV-VIS-NIR spectral range (Figure. 1c, black solid curve, monolayer $MoSe_2$) while featuring two low energy peaks which relate to the A_0 and B_0 excitons.[5-6, 12-13]

We combined atomically thin $MoSe_2$ with two strong light harvesting nanomaterials whose excitonic properties are chosen such that directional energy transfer can be promoted between themselves and with $MoSe_2$, respectively (see Figure. 1a-b). They are: (i) a water soluble colloidal core/shell CdSe/ZnS quantum dot (QD) emitting at around 585 nm[2-3] and (ii) a crosslinked allophycocyanin (APC), a trimeric disk-like shaped protein of about 11-nm diameter, 3nm thick and with a central channel of about 3.5nm and which is part of the light harvesting system of Cyanobacteria.[14] This trimeric protein incorporates, in each monomer, a dimeric phycocyanobilin chromophore, with all three dimers strongly coupled within the trimeric protein (Fig.1a, top view, chromophores are depicted as grey colored balls).[14-15] APC protein absorbs broadly at around 650 nm and emits with a sharp peak at 660 nm when dissolved in a neutral buffer (Figure. 1c).[9] When APC is combined with QDs, it forms a donor-acceptor Foerster-resonant energy transfer (FRET) pair for which the FRET rate can be expressed by[16]

$$\Gamma_{FRET} = \frac{9(ln10)k^2 \Phi_{QD}}{128\pi^5 N_{AV} n^4 \tau_{QD}^0 r^6} \times J(\lambda) \quad (1)$$

with Φ_{QD} and τ_{QD}^0 the PL quantum yield and the PL lifetime of the donor only component (QD), k^2 an orientation factor, N_{AV} the Avogadro number, r the donor (QD)-acceptor (APC) separation distance and $J(\lambda)$ the overlap integral between QD's PL spectrum and APC's absorption spectrum, which is given by

$$J(\lambda) = \int I_{QD}(\lambda) \times \varepsilon_{APC}(\lambda) \times \lambda^4 d\lambda \quad (2)$$

In this equation $\int I_{QD}(\lambda)d\lambda = 1$, with $I_{QD}(\lambda)$ the PL emission of the QD and $\varepsilon_{APC}(\lambda)$ the extinction spectrum of APC. According to eqs.1&2, both the QD and the APC protein feature very appealing light harvesting properties for promoting a strong FRET: high extinction coefficients, 1,900k $M^{-1}cm^{-1}$ for QD, 700k $M^{-1}cm^{-1}$ for APC, high quantum yields of photoluminescence (PL), 60% for QDs, 68% for APC, strongly coupled chromophores for APC and strong spectral overlap between QD's emission and APC absorption (Figure. 1c). This allows photoexcited QDs to transfer energy to APC proteins when part of a donor-acceptor QD-APC hybrid (FRET I, Fig.1c). Furthermore, APC protein has an emission spectrum which completely overlaps with $MoSe_2$'s absorption spectrum (Figure. 1c), thus being able to transfer to $MoSe_2$ nanosheet when both are combined in a hybrid (FRET-II, Fig.1c) and whether APC is photoexcited directly or via energy transfer. By assembling QDs, APC proteins and a $MoSe_2$ nanosheet onto a nanohybrid as shown in Figure 1a, with QDs residing at the outer side of the nanohybrid and APC proteins sandwiched between QDs and $MoSe_2$, a step-wise directional energy transfer can be achieved from photoexcited QDs to APC (FRET I, Fig.1a,1c) and finally to $MoSe_2$ (FRET II, Fig.1a,1c). In this same QD-APC-$MoSe_2$ hybrid, a direct transfer from photoexcited QDs to $MoSe_2$ (FRET III, Fig.1a,1c) will be inhibited by the large donor-acceptor separation provided with the intercalation of the protein and the length of the QD's capping ligands (Figure. 1a,1b). This designed step-wise directional energy transfer mimics the case of natural light harvesting systems where chromophores at the surface (here QDs) harvest light and physically displace the harvested energy to intermediate chromophores (here APC) and finally to the reaction center (here $MoSe_2$). The stepwise FRET will provide increased exciton density and enhanced charge carrier generation in the atomically thin $MoSe_2$.

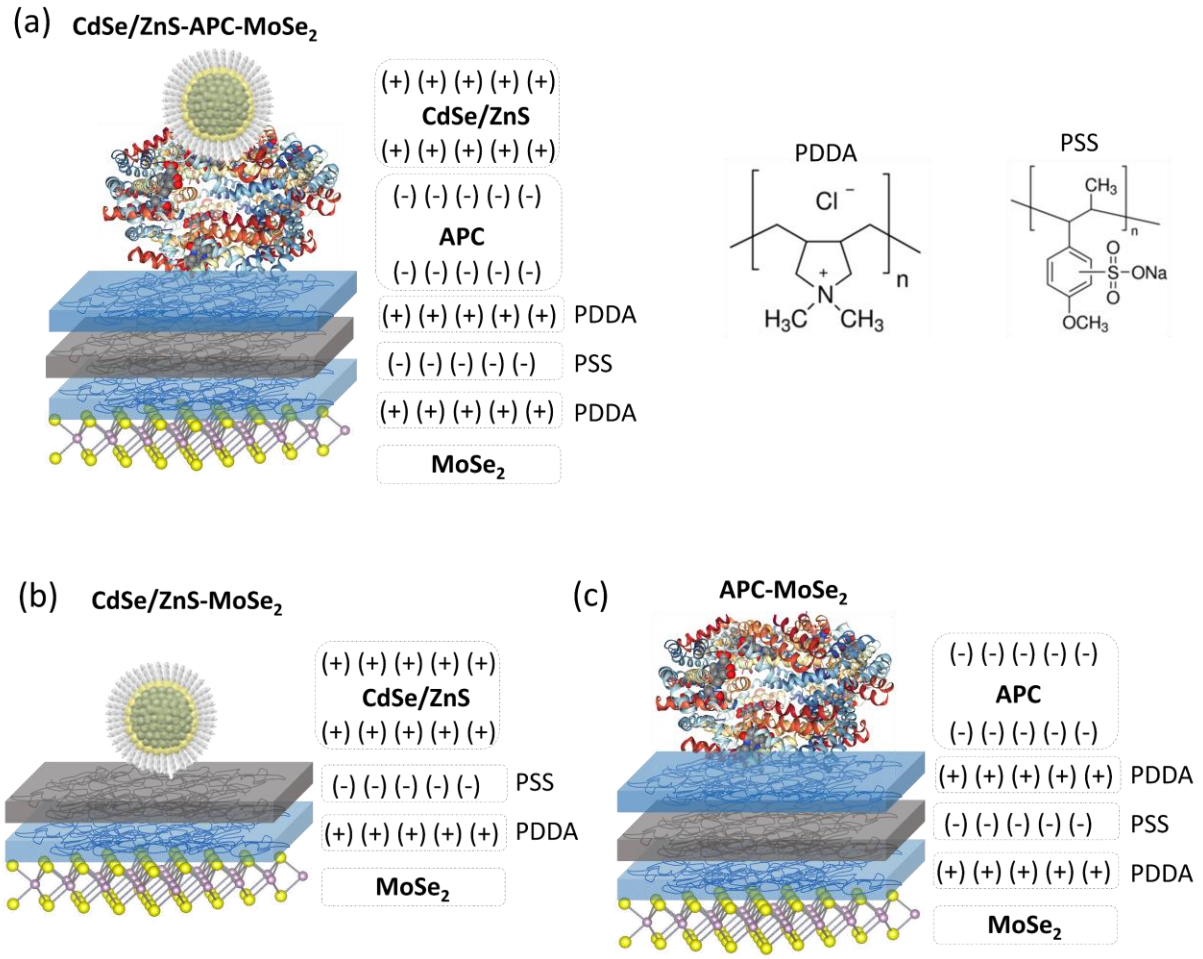

Figure. 2. Self-assembly strategy for the biotic-abiotic hybrid nanostructure incorporating 2D van Der Waals semiconductor. Hydrophobic layered $MoSe_2$ is hydrophilized by layer-by-layer polyelectrolyte deposition using poly(diallyl dimethyl ammonium chloride) (PDDS) and poly(styrene sulfonate) (PSS). The biotic/abiotic $MoSe_2$-APC-QD hybrid nanostructure (panel a) is assembled by depositing a negatively charged APC protein layer followed by deposition of positively charged (aminated polyethylene glycol coated) QDs. (b) and (c) are hybrid nanostructures composed of $MoSe_2$-QD and $MoSe_2$-APC, with $MoSe_2$ hydrophilized as described above.

To practically implement the design shown in Figure 1a, we used a layer-by-layer (LbL) deposition method to introduce hydrophilicity at the surface of the highly hydrophobic $MoSe_2$ flake to allow the assembly of negatively charged APC by electrostatic deposition. Figure 2 shows in detail each of the components constituting the biotic/abiotic hybrid nanostructure. We used two oppositely charged polyelectrolytes, poly(diallyl dimethyl ammonium chloride) (PDDA) and

poly(styrene sulfonate) (PSS), with the resulting polyelectrolyte layer having a thickness of 2-3 nm. We then incubated the hydrophilized $MoSe_2$ flake with a phosphate buffered solution containing APC (pH 7.4, APC's isoelectric point is 4.68). We then rinsed the unbound proteins, and finally incubated the APC-$MoSe_2$ nanohybrid with a solution of positively charged (amine functionalized) QDs followed by the rinse of unbound QDs. Having a monolayer of APC proteins physically sandwiched between a $MoSe_2$ nanosheet and a monolayer of QDs, the resulting QD-APC-$MoSe_2$ nanohybrid is expected to exhibit an energy flow physically oriented from QDs to APC and finally to $MoSe_2$, thus mimicking a natural light harvesting system.

We probed the energy transfer flow in the assembled $MoSe_2$-APC-QD nanohybrid by time-resolved confocal fluorescence microscopy (FLIM). We used a 440nm/532nm pulsed laser source (Picoquant, Germany, 75 picosecond pulses, 10 MHz repetition rate, average power of 10 nW at the sample). We excited QDs and QD-based hybrids using the 440nm light and probed the emission at around 580nm and we also excited APC and APC-$MoSe_2$ at 532nm and probed at around 660nm. Results of the confocal FLIM experiments are part of Figures 3 and 4, and Table 1. APC proteins and QDs deposited on Si/SiO_2 support exhibit PL lifetimes of 1.05 ns and 21.20 ns, respectively (Figures 3c, 3f, black colored curves and Table 1). Electrostatically assembled QD-APC hybrids on Si/SiO_2 substrate show QD's lifetime being quenched to 17.0 ns (Fig.4a, Table 1). This suggests the QD-APC hybrid exhibits a FRET rate, $k_{FRET} = 1/\tau_{hybrid} - 1/\tau_{donor}$=1.15x$10^7$ ns^{-1} and an efficiency $E_{FRET} = 1 - \tau_{hybrid}/\tau_{donor}$=20% (Table 1). This is a rather low efficiency value which we expected, given the large separation distance between QD and APC which is introduced by the QD's aminated polyethylene glycol (PEG) shell (5-6 nm thick according to the vendor, Ocean Nanotech), the presence of a ZnS shell (0.7 nm), plus the separation imposed by the protein scaffold having the chromophores buried inside (Fig.1a,

top view). Figure 3 shows correlative confocal reflection (Figure. 3a, 3d, 3g) and FLIM (Figure. 3b, 3e, 3h) images of $MoSe_2$ flakes doped with monolayer QD (Figure. 3a, 3b), monolayer APC protein (Figure.3d, 3e), and bilayer APC-QD (Figure. 3g, 3h), respectively. FLIM images were recorded at the emission spectral range of the donor moiety (for QD @580nm, for APC @680nm). Reflection images identify single-, two- and three-layers (red, green and blue dots), and these were confirmed by atomic force microscopy (AFM) measurements (Figure. S1, supporting information, SI). FLIM images in Fig.3 show strong photoluminescence (PL) quenching for QD, APC and QD-APC components deposited on $MoSe_2$ flakes vs components on Si/SiO_2 support (Figs.3b,3e,3h, regions adjacent to flakes). The same FLIM images show increase in PL quenching of QD, APC and APC-QD components with increased number of $MoSe_2$ layers, e.g. from monolayer to few layers.

To quantify the observed PL quenching vs number of $MoSe_2$ monolayers, we performed diffraction limited (point) time-resolved measurements and the results of these experiments are shown in Figures 3c, 3f, and 3i, Figure 4 and Table 1. PL decays recorded from all three types of hybrids, QD-$MoSe_2$ (Figure. 3c), APC-$MoSe_2$ (Figure. 3f) and QD-APC-$MoSe_2$ (Figure. 3i), they all show increased quenching with added number of $MoSe_2$ layers. FRET rates and efficiencies were calculated as $k_{FRET} = 1/\tau_{hybrid} - 1/\tau_{donor}$ and $E_{FRET} = 1 - \tau_{hybrid}/\tau_{donor}$. Here we considered PL lifetimes of donor only (τ_{donor}) those measured from monolayer QDs deposited on Si/SiO_2, (440nm excitation, 580nm emission) and of monolayer APC deposited on Si/SiO_2, (532nm excitation, 680nm emission). PL lifetimes of hybrids (τ_{hybrid}) where those measured from QDs on $MoSe_2$ (440nm excitation, 580nm emission), APC on $MoSe_2$ (532nm excitation, 660nm emission), and QD-APC on $MoSe_2$ (440nm excitation, 580nm emission).

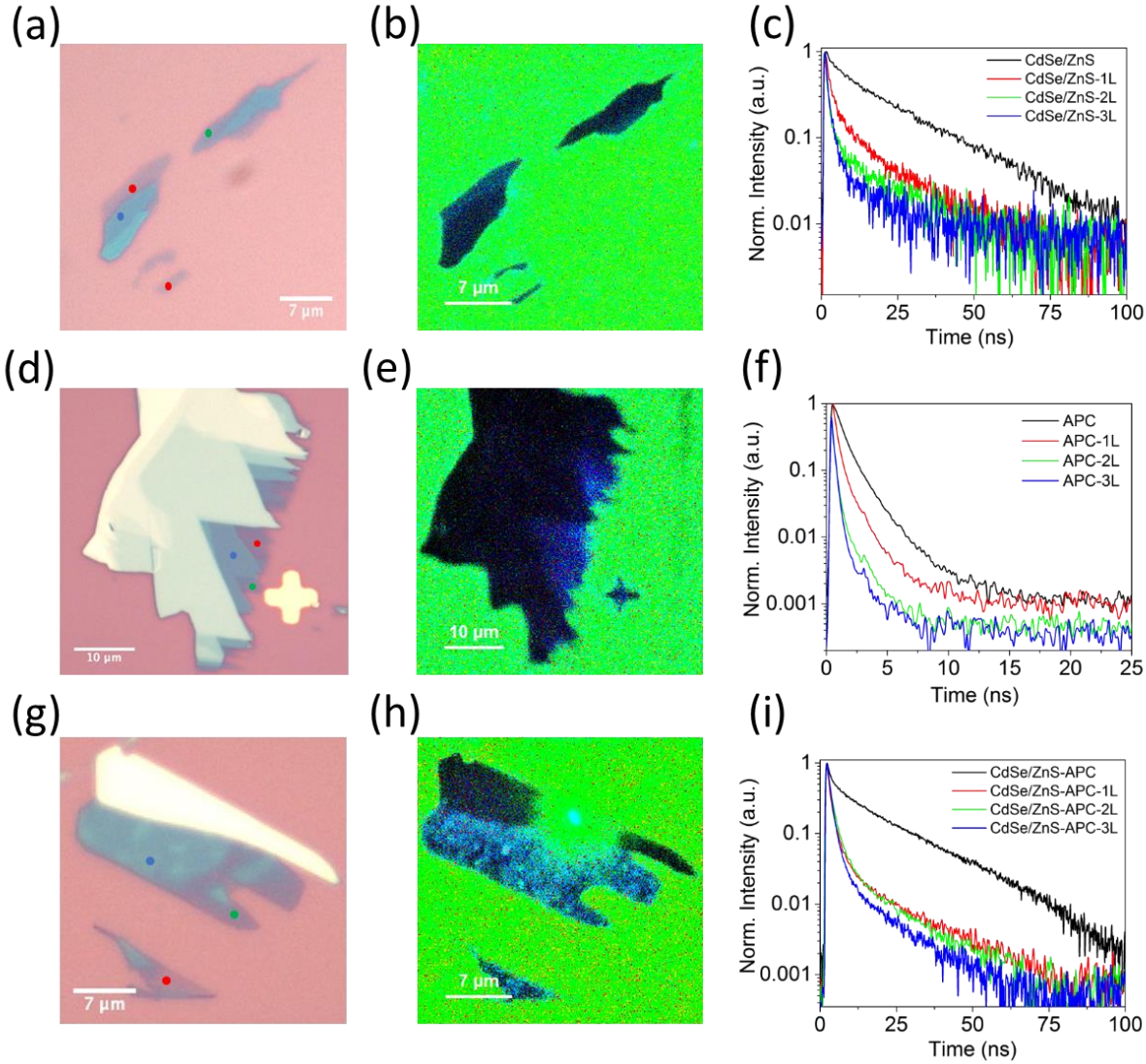

Figure 3. (a)-(b), (d)-(e), and (g)-(h) are correlated optical reflection and confocal FLIM images of QD-$MoSe_2$, APC-$MoSe_2$, and QD-APC-$MoSe_2$ hybrids, respectively. Single-, two- and three-layer $MoSe_2$ are indicated by red, green and blue dots. (c) and (f) and (i) are diffraction-limited photoluminescence decays of QD-$MoSe_2$, APC-$MoSe_2$ and QD-APC-$MoSe_2$ hybrids vs number of $MoSe_2$ layers. 1L, single layer, 2L, bilayer, 3L, tri-layer.

From 1-layer $MoSe_2$ up to 3-layers $MoSe_2$ we observed that the FRET efficiency increased from 20% to 38% for the APC-$MoSe_2$ hybrid, from 38% to 71% for the QD-$MoSe_2$ hybrid and from 68% to 84% for the QD-APC-$MoSe_2$ hybrid (Table 1). It is noteworthy that out of the three monolayer $MoSe_2$ based hybrids, the biotic-abiotic QD-APC-$MoSe_2$ hybrid outperforms in transferred energy the QD-$MoSe_2$ hybrid (Fig.4a, QD-APC-$MoSe_2$ decay vs QD-APC-$MoSe_2$

decay, and Table 1), thus suggesting APC helps with improving the transfer of energy from QDs to $MoSe_2$. The insertion of an additional step in the energy transfer from QD to $MoSe_2$ is expected to decrease the overall efficiency of the transfer, since both QD-APC (FRET I) and APC-$MoSe_2$ (FRET II) steps proceed with less that 100% efficiency. However, our FLIM data prove otherwise. Recent work has shown that light harvesting systems with highly ordered chromophores can act as energy funnels, dramatically increasing the transfer with external acceptors.[17-18] We propose a similar phenomenon to take place here where APC proteins added between QDs and $MoSe_2$ nanosheet can enhance the FRET from QD to $MoSe_2$ via a "funnel-like" effect. APC's small isoelectric point value makes the protein negatively charged at neutral pH and APC's disk-like shape will align the protein gn parallel to the surface of $MoSe_2$ when binding to the polyelectrolytes. In this scenario, the multiple chromophores buried inside protein's cage will align their dipoles parallel to $MoSe_2$ which also has an in plane dipole. Because QDs have a degenerate dipole moment with no preferential orientation like it is usually found in organic chromphores,[19] the energy transfer in QDs-$MoSe_2$ and in QD-APC pairs is rather weak, in particular in our case where QDs have a rather thick shell (>5nm) and space themselves at large distances from the acceptor, either APC or $MoSe_2$. Intercalating APC in between QDs and $MoSe_2$ can create a funnel-like effect leading to an enhanced transfer of the energy from the QDs onto the MoSe2 via APC. While speculative, this model will require theoretical support in the future.

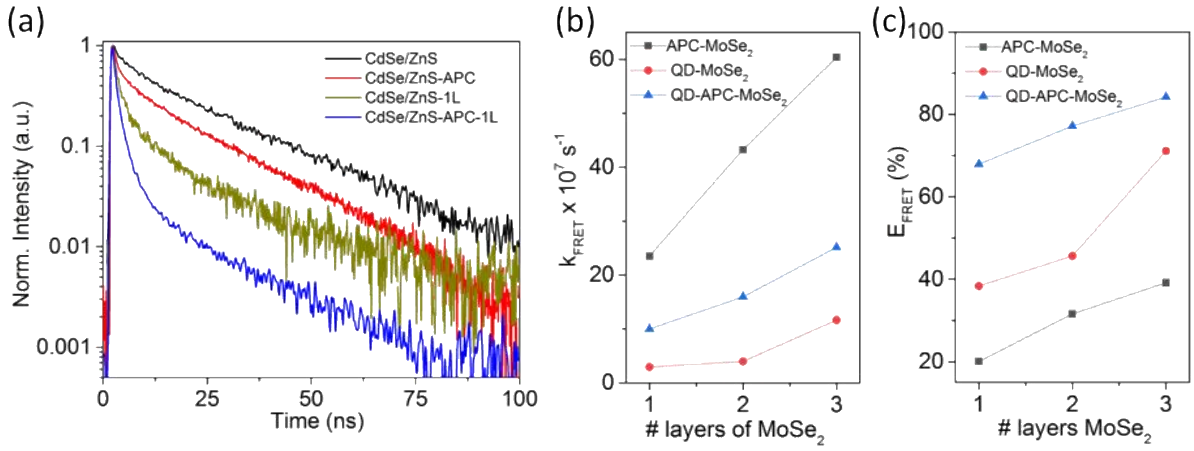

Figure 4. (a) photoluminescence decays of QDs on SiO_2/Si substrate, of QD-APC hybrids, of QD-1L-$MoSe_2$ hybrids, and of QD-APC-1L $MoSe_2$ hybrids. FRET rates (b) and efficiencies (c) vs number of layers of $MoSe_2$ for APC-$MoSe_2$ (black line and square), QD-$MoSe_2$ (red line and dots) and QD-APC-$MoSe_2$ (blue line and triangles). See text for computation of FRET rates.

From bulk to monolayer, $MoSe_2$ changes its energy bandgap from indirect to direct semiconductor, similar as it does MoS_2.[5, 8] For MoS_2, its combination with QDs resulted in QD-MoS_2 hybrids with layer dependent energy transfer, with single layer MoS_2 exhibiting the strongest quenching for QDs.[20-21] This trend in FRET rate with number of MoS_2 layers was attributed to a dielectric screening of the electric field of the QD's emitting dipole by the addition of extra layers, next to the monolayer MoS_2, which in turn weakens the FRET rate. As such, the strongest FRET is to be observed with monolayer MoS_2. Oppositely, graphene and indirect bandgap layered metal dichalcogenides like SnS_2 were found to exhibits an increase in FRET rate from monolayer and thicker, possible due to a weaker dielectric screening by added monolayers.[21-22] However, here we observed a similar layer dependency of the FRET rate for both QDs and APC interacting with layered $MoSe_2$ as it was previously reported for QDs transferring to graphene and to SnS_2, yet opposite to that of QDs deposited on layered MoS_2. To account for an eventual effect of the polyelectrolytes used to hydrolyze $MoSe_2$, we performed confocal FLIM experiments with amine-capped CdSe/ZnS QDs deposited directly on $MoSe_2$ flakes as well on MoS_2 flakes (Table S1, SI).

For MoS_2 we obtained a similar trend for the FRET rate vs number layers of MoS_2 as shown in previous reports and with the strongest FRET observed for monolayer MoS_2.[20-21] However, our observed FRET rate for CdSe/ZnS QDs transferring to monolayer MoS_2 (Table S1, SI) is 4x weaker than previously reported.[20] We believe this difference results from the presence of an aminated polyethylene glycol shell coating the QDs, with a thickness of 5-6 nm (as provided by the manufacturer, Ocean Nanotech), which acts as an additional spacer for QDs transferring to monolayer MoS_2, thus slowing down the FRET when compared with the use of QDs with short organic ligands.[20] For $MoSe_2$ we obtained a similar trend as that shown in Figure 4b,c, thus concluding that the LBL polyelectrolyte intercalated between $MoSe_2$ and QDs and APC proteins had no influence on the trend of the FRET rate vs number layers of $MoSe_2$, rather than that of a physical spacer. One possible explanation for the observed differences between the FRET transfer of QDs to MoS_2 and $MoSe_2$ is provided below. The FRET rate of QDs transferring to $MoSe_2$ depends upon the dielectric constant of the 2D material which, in a simplistic picture, can be written as $k_{FRET} \sim \varepsilon_2 \int V dV \, |\mathbf{E}|^2$, with V the volume of the 2D material and $\varepsilon = \varepsilon_1 + i * \varepsilon_2$ the dielectric function of the 2D material.[21] A recent report identifies monolayer MoS_2 to exhibit a larger imaginary component for the dielectric function vs monolayer $MoSe_2$.[23] The larger atomic mass and therefore bulkiness of Selenium vs Sulphur might account for a larger interlayer separation as seen by AFM measurements (see Fig.S1, SI) which could lead to weaker interaction between atomically thin layers in the case of $MoSe_2$ vs MoS_2. This might be the reason of reduced dielectric screening from underneath layers. As such, each $MoSe_2$ monolayer would function as an independent energy acceptor with the donor, thus providing an opposite trend for FRET rate vs number of layers for the two types of hybrids.

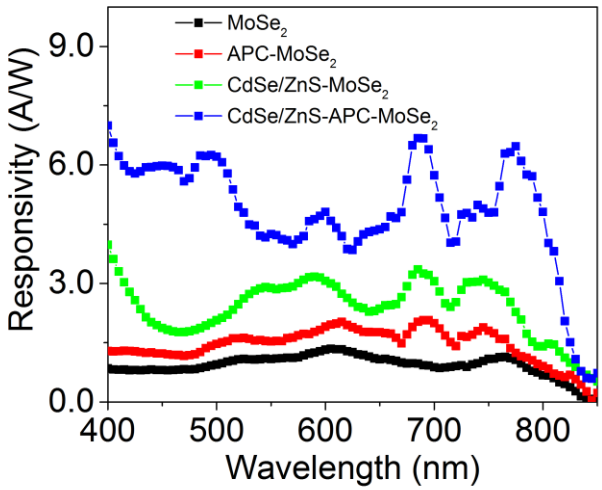

Figure 5. Spectral responsivity of pristine $MoSe_2$, CdSe/ZnS-$MoSe_2$, APC-$MoSe_2$ and CdSe-APC-$MoSe_2$ field effect transistors, showing best responsivity for the biotic/abiotic hybrid FET.

Finally, to demonstrate the improvement in photoresponse following the biotic/abiotic hybrid design and assembly, we fabricated field effect transistors from $MoSe_2$ flakes exfoliated on Si/SiO_2 support, with source and drain electrodes constructed by electron beam lithography and as detailed in supporting information section. Figure 5 shows spectral photoresponsivities measured from pristine and hybrid devices, including the biotic-abiotic hybrid device which outperforms in photoresponsivity of the pristine ($MoSe_2$ only) FET, APC-$MoSe_2$ FET and the all-inorganic QD-$MoSe_2$ FETs, especially in the visible and near infrared spectral regions.

In conclusion, we assembled a biotic-abiotic hybrid nanosystem following architectural inspiration from nature's light harvesting systems and utilizing an atomically thin transition metal dichalcogenide nanosheet as a support for the bottom-up assembly of the proposed hybrid. Through self-assembly and bandgap engineering, we obtained a cascaded step-wise directional energy transfer leading to improved light harvesting and exciton and charge carrier density production as demonstrated by optical and photoelectrical measurements. Judging from the dimensions of the components involved in defining the biotic-abiotic nanohybrid, 5-6nm for the

amine terminated PEG shell, the ZnS shell (1nm), the APC protein (3nm thick) and the LBL layer (2-3nm), we estimate a physical move of the excitation energy transfer from QDs to $MoSe_2$ through the APC motif of 12-20nm. We believe this is one of the first demonstration of a cascaded biotic-abiotic nanohybrid involving a 2D van Der Waals semiconductor. Finally, we observed different trends for energy transfer rate vs layer number in two transition metal dichalcogenide semiconductors which both exhibit bandgap inversion, $MoSe_2$ vs MoS_2 and reasoned that such difference might arise from differences in dielectric function as well in chalcogenide bulkiness.

Acknowledgments. This work was carried out at the Center for Functional Nanomaterials, Brookhaven National Laboratory (BNL), which is supported by the U.S. Department of Energy, Office of Basic Energy Sciences, under Contract No. DE-SC0012704.

Table 1. Photoluminescence lifetimes, FRET rates and FRET efficiencies for isolated components and various hybrids, including the biotic-abiotic QD-APC-MoSe2 hybrid. 1L, 2L, 3L denotes 1, 2 and 3 atomically thin layers of MoSe2 and hybrids composed of MoSe2. All time-resolved data were detected at the emission peak of QD (585nm), except for APC (680nm) and MoSe2 (800nm). Lifetimes are presented as amplitude averaged following 2- or 3-exponent fits (see details of analysis in SI).

Sample	**PL lifetime /ns**	**k_{FRET} x10^7 /s^{-1}**	**E_{FRET} /%**
Donor and acceptor separated components			
CdSe/ZnS QD on Si/SiO_2	21.20	-	-
APC on Si/SiO_2	1.07	-	-
$MoSe_2$	<0.08	-	-
QD-APC hybrid			
QD-APC	17.02	1.158	20
APC-$MoSe_2$ hybrid			
APC-1L MoSe2	0.85	23.51	20
APC-2L MoSe2	0.73	43.27	32
APC-3L MoSe2	0.65	60.36	39
QD-$MoSe_2$ hybrid			
QD-1L MoSe2	13.07	2.93	38
QD-2L MoSe2	11.52	3.96	46
QD-3L MoSe2	6.12	11.62	71
QD-APC-$MoSe_2$ hybrid			
QD-APC-1L MoSe2	6.80	9.99	68
QD-APC-2L MoSe2	4.84	15.94	77
QD-APC-3L MoSe2	3.35	25.13	84

References

1. Scholes, G. D.; Fleming, G. R.; Olaya-Castro, A.; Van Grondelle, R., Lessons from nature about solar light harvesting. *Nature chemistry* **2011,** *3* (10), 763.
2. Loos, D.; Cotlet, M.; De Schryver, F.; Habuchi, S.; Hofkens, J., Single-molecule spectroscopy selectively probes donor and acceptor chromophores in the phycobiliprotein allophycocyanin. *Biophysical journal* **2004,** *87* (4), 2598-2608.
3. Ying, L.; Xie, X. S., Fluorescence spectroscopy, exciton dynamics, and photochemistry of single allophycocyanin trimers. *The Journal of Physical Chemistry B* **1998,** *102* (50), 10399-10409.
4. Collini, E.; Wong, C. Y.; Wilk, K. E.; Curmi, P. M.; Brumer, P.; Scholes, G. D., Coherently wired light-harvesting in photosynthetic marine algae at ambient temperature. *Nature* **2010,** *463* (7281), 644.
5. Tonndorf, P.; Schmidt, R.; Böttger, P.; Zhang, X.; Börner, J.; Liebig, A.; Albrecht, M.; Kloc, C.; Gordan, O.; Zahn, D. R., Photoluminescence emission and Raman response of monolayer MoS 2, MoSe 2, and WSe 2. *Optics express* **2013,** *21* (4), 4908-4916.
6. Mak, K. F.; Lee, C.; Hone, J.; Shan, J.; Heinz, T. F., Atomically Thin MoS2: A New Direct-Gap Semiconductor. *Physical Review Letters* **2010,** *105* (13), 136805.
7. Huang, Y.; Sutter, E.; Sadowski, J. T.; Cotlet, M.; Monti, O. L.; Racke, D. A.; Neupane, M. R.; Wickramaratne, D.; Lake, R. K.; Parkinson, B. A., Tin Disulfide · An Emerging Layered Metal

Dichalcogenide Semiconductor: Materials Properties and Device Characteristics. *Acs Nano* **2014,** *8* (10), 10743-10755.
8. Splendiani, A.; Sun, L.; Zhang, Y.; Li, T.; Kim, J.; Chim, C.-Y.; Galli, G.; Wang, F., Emerging Photoluminescence in Monolayer MoS2. *Nano Letters* **2010,** *10* (4), 1271-1275.
9. Yeh, S. W.; Ong, L. J.; Glazer, A. N.; Clark, J. H., Fluorescence properties of allophycocyanin and a crosslinked allophycocyanin trimer. *Cytometry: The Journal of the International Society for Analytical Cytology* **1987,** *8* (1), 91-95.
10. Dabbousi, B. O.; Rodriguez-Viejo, J.; Mikulec, F. V.; Heine, J. R.; Mattoussi, H.; Ober, R.; Jensen, K. F.; Bawendi, M. G., (CdSe)ZnS Core−Shell Quantum Dots: Synthesis and Characterization of a Size Series of Highly Luminescent Nanocrystallites. *The Journal of Physical Chemistry B* **1997,** *101* (46), 9463-9475.
11. Liu, J.-Y.; Jiang, T.; Zhang, J.-P.; Liang, D.-C., Crystal structure of allophycocyanin from red AlgaePorphyra yezoensis at 2.2-Å resolution. *Journal of Biological Chemistry* **1999,** *274* (24), 16945-16952.
12. Yuan, L.; Wang, T.; Zhu, T.; Zhou, M.; Huang, L., Exciton dynamics, transport, and annihilation in atomically thin two-dimensional semiconductors. *The journal of physical chemistry letters* **2017,** *8* (14), 3371-3379.
13. Chen, S.-Y.; Zheng, C.; Fuhrer, M. S.; Yan, J., Helicity-resolved Raman scattering of MoS2, MoSe2, WS2, and WSe2 atomic layers. *Nano letters* **2015,** *15* (4), 2526-2532.
14. Brejc, K.; Ficner, R.; Huber, R.; Steinbacher, S., Isolation, crystallization, crystal structure analysis and refinement of allophycocyanin from the cyanobacterium Spirulina platensis at 2.3 Å resolution. *Journal of molecular biology* **1995,** *249* (2), 424-440.
15. Edington, M. D.; Riter, R. E.; Beck, W. F., Evidence for coherent energy transfer in allophycocyanin trimers. *The Journal of Physical Chemistry* **1995,** *99* (43), 15699-15704.
16. Clapp, A. R.; Medintz, I. L.; Mattoussi, H., Förster resonance energy transfer investigations using quantum‐dot fluorophores. *ChemPhysChem* **2006,** *7* (1), 47-57.
17. Camacho, R.; Tubasum, S.; Southall, J.; Cogdell, R. J.; Sforazzini, G.; Anderson, H. L.; Pullerits, T.; Scheblykin, I. G., Fluorescence polarization measures energy funneling in single light-harvesting antennas—LH2 vs conjugated polymers. *Scientific reports* **2015,** *5*, 15080.
18. Pieper, A.; Hohgardt, M.; Willich, M.; Gacek, D. A.; Hafi, N.; Pfennig, D.; Albrecht, A.; Walla, P. J., Biomimetic light-harvesting funnels for re-directioning of diffuse light. *Nature communications* **2018,** *9* (1), 666.
19. Patra, D.; Gregor, I.; Enderlein, J.; Sauer, M., Defocused imaging of quantum-dot angular distribution of radiation. *Applied Physics Letters* **2005,** *87* (10), 101103.
20. Prins, F.; Goodman, A. J.; Tisdale, W. A., Reduced Dielectric Screening and Enhanced Energy Transfer in Single- and Few-Layer MoS2. *Nano Letters* **2014,** *14* (11), 6087-6091.
21. Raja, A.; Montoya−Castillo, A.; Zultak, J.; Zhang, X.-X.; Ye, Z.; Roquelet, C.; Chenet, D. A.; van der Zande, A. M.; Huang, P.; Jockusch, S.; Hone, J.; Reichman, D. R.; Brus, L. E.; Heinz, T. F., Energy Transfer from Quantum Dots to Graphene and MoS2: The Role of Absorption and Screening in Two-Dimensional Materials. *Nano Letters* **2016,** *16* (4), 2328-2333.
22. Zang, H.; Routh, P. K.; Huang, Y.; Chen, J.-S.; Sutter, E.; Sutter, P.; Cotlet, M., Nonradiative Energy Transfer from Individual CdSe/ZnS Quantum Dots to Single-Layer and Few-Layer Tin Disulfide. *ACS Nano* **2016,** *10* (4), 4790-4796.

23. Li, Y.; Chernikov, A.; Zhang, X.; Rigosi, A.; Hill, H. M.; van der Zande, A. M.; Chenet, D. A.; Shih, E.-M.; Hone, J.; Heinz, T. F., Measurement of the optical dielectric function of monolayer transition-metal dichalcogenides: MoS 2, Mo S e 2, WS 2, and WS e 2. *Physical Review B* **2014,** *90* (20), 205422.
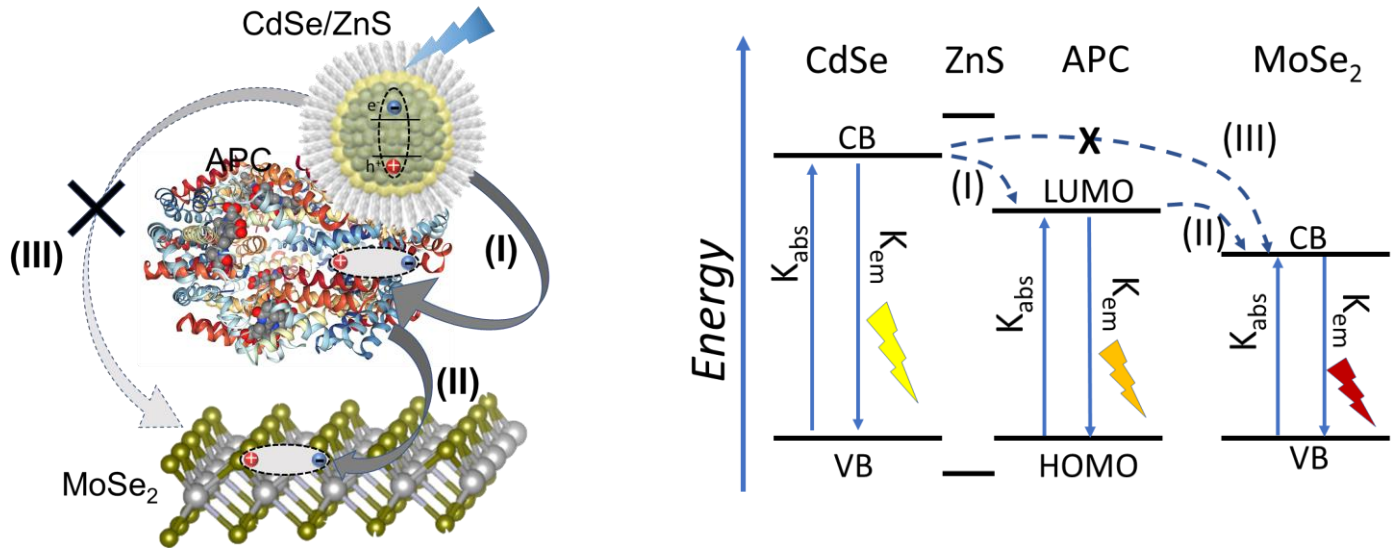
TOC